한국대기환경학회지 제 26 권 제 5 호
J. KOSAE Vol. 26, No. 5 (2010) pp. 475～489
Journal of Korean Society for Atmospheric Environment

Enhancement of Ozone and Carbon Monoxide Associated with Upper Cut-off Low during Springtime in East Asia

Yun Seob Moon* and James R. Drummond[1)]
Department of Environmental Education, Korea National University of Education, Cheongwon, Korea
[1)]*Department of Physics, University of Toronto, Canada*

(Received 21 September 2009, revised 16 July 2010, accepted 3 September 2010)

Abstract

In order to verify the enhancement of ozone and carbon monoxide (CO) during springtime in East Asia, we investigated weather conditions and data from remote sensors, air quality models, and air quality monitors. These include the geopotential height archived from the final (FNL) meteorological field, the potential vorticity and the wind velocity simulated by the Meteorological Mesoscale Model 5 (MM5), the back trajectory estimated by the Hybrid Single-Particle Lagrangian Integrated Trajectory (HYSPLIT) model, the total column amount of ozone and the aerosol index retrieved from the Total Ozone Mapping Spectrometer (TOMS), the total column density of CO retrieved from the Measurement of Pollution in the Troposphere (MOPITT), and the concentration of ozone and CO simulated by the Model for Ozone and Related Chemical Tracers (MOZART). In particular, the total column density of CO, which mightoriginate from the combustion of fossil fuels and the burning of biomass in China, increased in East Asia during spring 2000. In addition, the enhancement of total column amounts of ozone and CO appeared to be associated with both the upper cut-off low near 500 hPa and the frontogenesis of a surface cyclone during a weak Asian dust event. At the same time, high concentrations of ozone and CO on the Earth's surface were shown at the Seoul air quality monitoring site, located at the surface frontogenesis in Korea. It was clear that the ozone was invaded by the downward stretched vortex anomalies, which included the ozone-rich airflow, during movement and development of the cut-off low, and then there was the catalytic photochemical reaction of ozone precursors on the Earth's surface during the day. In addition, air pollutants such as CO and aerosol were tracked along both the cyclone vortex and the strong westerly as shown at the back trajectory in Seoul and Busan, respectively. Consequently, the maxima of ozone and CO between the two areas showed up differently because of the time lag between those gases, including their catalytic photochemical reactions together with the invasion from the upper troposphere, as well as the path of their transport from China during the weak Asian dust event.

Key words : Total column density of CO, Total column amounts of ozone, Upper cut-off low, Vortex anomalies, Catalytic chemical reaction

* Corresponding author.
Tel : +82-10-9323-4117, E-mail : ysmoon@knue.ac.kr

1. INTRODUCTION

The oxidation of CO in the presence of NO_x is directly related to ozone production as ozone precursors in the troposphere. Correlation between CO and ozone is strong and consistently negative due to titration of ozone by NO (Cardenas *et al*., 1998).

CO is more concentrated in the troposphere, with much lower concentrations in the stratosphere (Pan *et al*., 1998; Cicerone, 1988). The major sources of CO are the oxidation of CH_4 via formaldehyde (HCHO), biomass burning, oxidation of hydrocarbons (mainly natural), and fossil fuel combustion (Warneck, 2000). The main sink of CO is OH oxidation to CO_2, and its smaller sink is consumed by soils or transported to the stratosphere (Hobbs, 2000). The large variability in the global tropospheric CO budget is mainly associated with the variability of global distribution of tropospheric hydroxyl (OH). Jacob (1999) reported that CO in the troposphere could be oxidized by the OH molecules originating from ozone transported across the tropopause. Wang *et al.* (1999) also indicated that the increased CO could indirectly intensify global warming and perturb the stratospheric ozone through stratosphere and troposphere exchange (STE) by increasing the lifetimes of trace gases such as CH_3Cl and CH_3CCl_3. In general, CO and ozone (O_3) can be used as excellent tracers for studies on long-range transport, convection, and STE of air pollutants. For example, CO in models of global CO budgets has been estimated to have an average atmospheric lifetime of approximately weeks or two months (Warneck, 1988).

The exchange of chemical species between the stratosphere and troposphere may play an important role in atmospheric chemistry. In order to assess enhancements of O_3 and CO during springtime in East Asia, STE has to be well understood, as it is due to tropopause folding in the rear of the upper jet streak, the strongest mean westerly within the jet stream. For example, the downward transport from the stratosphere presents a significant source of tropospheric ozone and constitutes the removal mechanism for many stratospheric species, including ozone depletion (Seinfeld and Pandis, 1998). The STE of ozone-rich air occurs in weather conditions of the cut-off low related to the polar and subtropical jet stream at mid-latitudes (Cooper *et al*., 1998; Astin and midgley, 1994; Davies and Schuepbach, 1994). In particular, Kim *et al*. (2002) reported that the enhancement of ozone and aerosol over Korea during Asian dust events occurred in the presence of the upper cut-off low and the surface high pressure system. Kondratyev and Varotsos (2000) observed also a sharp tropospheric ozone increase due to the cross-tropopause exchange. Of course, it is important to understand the vertical structure between the long-range transport of tropospheric CO and the STE of ozoneunder such weather conditions. But there still remain many uncertainties from a limited number of studies on the STE of ozone-rich air. Therefore, it is essential to investigate the spatial distribution of O_3 and CO concentrations from remote sensing and air quality model data, as well as the model data together with synoptic weather conditions.

Many research groups have been conducting O_3 and CO measurements to investigate long-term effects using ground-based and airborne instruments (Cardenas *et al*., 1998; Yurganov *et al*., 1997, 1995; Khalil and Rasmussen, 1994; Novelli *et al*., 1994; Tompson *et al*., 1994; Hubler *et al*., 1992; Marenco *et al*., 1989). These measured data have also been managed by a global surface O_3 and CO monitoring network, the Climate Monitoring and Diagnostic Laboratory of the National Oceanic and Atmospheric Administration Cooperative Air Sampling Network (NOAA CASN/CMDL, http://www.cmdl.noaa.gov/ccg/flask/sites.html). Additionally, we need to monitor the variation of total column amounts of ozone and CO on a global scale from satellite remote sensing. The data for amount of total ozone have been mainly obtained with the Total Ozone Mapping Spectrometer (TOMS, http://toms.gsfc.nasa.gov/aerosols/aerosols.html) instrument on board the Nimbus-7 satellite since late 1978. Four TOMS instruments have been sent into space: Nimbus-7 (1978～1993), Meteor-3 (1991～1994), ADEOS (1996～1997), and Earth Probe (1996-present). These TOMS instruments have provided excellent data for total ozone

amount and aerosol index (Fioletov *et al*., 1999). The total ozone amount is retrieved by viewing the backscattered ultraviolet albedo from the underlying surface and atmosphere in the Huggins band (from 310 nm to 350 nm) of the ozone absorption spectrum.

The satellite measurement of CO has been made by the Measurement of Air Pollution from Satellites (MAPS) instrument. MAPS has flown on the space shuttle on four occasions (http://www.stomy.larc.gov) and has provided global measurements (Reichle and Coauthors, 1999; Reichle *et al*., 1990). It is, however, limited in term of spatial resolution, vertical resolution and temporal extent. That is, there was a great need for long-term high resolution measurements of tropospheric CO. A new instrument known as the Measurement of Pollution in the Troposphere (MOPITT) provides such a data set. In particular, MOPITT is a nadir-viewing eight-channel infrared spectroscopy on board the Earth Observing System (EOS) Terr spacecraft in 1999. Its main objectives are to retrieve profiles and total column densities of CO and CH_4 (http://www.atmosp.physics.utoronto.ca/MOPITT/home.html). The retrieved total CO densities can anticipate an accuracy of 10 percent (Warner *et al*., 2001).

Recently, we have found an enhancement during springtime in East Asia from spatial distribution of the total CO amount retrieved by MOPITT. At the same time, we discovered that the total ozone amount retrieved by TOMS was also shown under special weather conditions. Therefore, the purpose of this study is to briefly describe the spatial characteristics of total CO densities retrieved by MOPITT, and then to verify the enhancement of CO and O_3 in East Asia (especially in Korea) using air quality modeling data as well as ground-based and satellite data under the weather conditions.

2. DATA AND INSTRUMENTS

The TOMS instrument for total ozone amount and aerosol index is used in this study to detect temporal and spatial distribution of ozone and aerosols. Furthermore, to verify the enhancement of ozone and CO on the Earth's surface, time series of ozone and CO were derived by using ultraviolet photometry and gas filter correlation radiometer, respectively, during the period of May 2000 at Busan (35.23˚N, 129.07˚E) and Seoul (37.5˚N, 127.0˚E) in Korea. The technique and types of the measurement are introduced by http://www.dasibi.com. These Dasibi models for air quality monitoring instrumentation are DASIBI 1008-AH for ozone and DASIBI 3008 for carbon monoxide. The accuracy of these Dasibi instruments has also been maintained during the measurement of air quality (http://www.dasibi.com). Relative uncertainty in the atmospheric concentrations obtained by the commercial equipment in routine analysis is estimated to be less than 5%.

To understand the sudden enhancement of total CO densities in East Asia during spring 2000, the MOPITT instrument data were also used. This instrument orbits the earth in a near-polar sun-synchronous configuration at approximately 700 km. The nadir viewing MOPITT instrument is an eight-channel gas correlation radiometer that measures CO profiles from terrestrial thermal radiation in the spectral region near 4.7 μm and total column densities of CO and CH_4 from reflected solar radiation in the spectral region near 2.3 μm and 2.2 μm, respectively (Warner, 2001). The MOPITT instrument makes use of two methods to modulate the transmittance in the gas cell: the cell pressure through the pressure-modulated cell (PMC) and the cell length through a length-modulated cell (LMC) (Drummond and Mand, 1996). These moulted radiometers, which include two PMCs and two LMCs for measurement of the CO profile and two LMCs each for total column densities of CO and CH_4, result in eight separate spectral channels by separating the 2- and 4.7 μm chennels after monochromatic radiation is filtered by the gas cell tansmission fuction. Consequently, the MOPITT instrument measures outgoing thermal emission from the atmosphere and surface in the thermal channels (1, 3, 5 and 7), and reflected solar radiation in the solar channels (2, 4, 6 and 8; channels 4 and 8 are CH_4 solar channels) that has passed through the atmosphere, been reflected on the surface, and transmitted back up through the atmosphere. Each channel pro-

duces an average signal, which represents mainly the background radiance (including Earth's surface and cloud characteristics), and a differential signal, which is more sensitive to atmospheric CO and CH_4 changes (Pan *et al*., 1995). In the solar channels related to total CO densities, the difference signals are sensitive to the absorption by CO as well as the solar intensity and surface reflectivity by solar radiation, and the average signals are sensitive to the solar intensity and surface reflectivity. Total CO densities are obtained by taking ratios of the difference signals to the average signals, which depend only on the absorption by CO. The retrieved total CO densities have the MOPITT pixels, 22×22 km in size, and can anticipate 10% precision (Warner *et al*., 2001; Wang *et al*., 1999; Pan *et al*., 1998). More detail MOPITT instruments are summarized by http://www.atmosp.physics.utoronto.ca/MOPITT/home.html.

3. SPATIAL DISTRIBUTION OF TOTAL CO COLUMN FROM MOPITT INSTRUMENT

Many standard retrieval techniques from the MOPITT instrument have mainly been introduced to retrieve the CO and CH_4 profiles (Warner *et al*., 2001;Wang *et al*., 1999; Pan *et al*., 1998). Consequently, the standard MOPITT retrieval outputs include CO mixing ratios at surface, 850 hPa, 700 hPa, 500 hPa, 350 hPa, 250 hPa and 150 hPa, surface temperature, surface thermal channel emissivity, and error variance of each of these variables. However, a defect of the retrieval technique for CO profiles is that it is difficult to determine the concentration in the boundary layer. This deficiency can be overcome by measuring total CO densities using the scattered sunlight from the surface in the 4285/cm band of CO (channel 2 and 6). The MOPITT CO retrieval algorithm is based on the maximum likelihood method. The optimal estimation method of trace gases can be used as follows (Rodgers, 1976): $\mathbf{X}_{n+1}=\mathbf{X}_a+\mathbf{S}_X\mathbf{K}_n^T\mathbf{K}_n\mathbf{S}_X\mathbf{K}_n^T+\mathbf{S}_\varepsilon[\mathbf{Y}-\mathbf{Y}_n-\mathbf{K}_n(\mathbf{X}_a-\mathbf{X}_n)]$, $\mathbf{S}=(\mathbf{S}_X^{-1}+\mathbf{S}_\varepsilon^{-1})^{-1}$, where $\mathbf{X}_n$ is the estimated atmospheric CO column vector at iteration n, $\mathbf{X}_a$ is the a priori (or background) CO information vector, $\mathbf{Y}_n$ is the calculated radiance signal vector at $\mathbf{X}_a$ given by forward model, $\mathbf{F(X)}$. $\mathbf{K}$ $(=\partial\mathbf{F}/\partial\mathbf{X})$ is the weighting function matrix, which can be calculated either analytically or by a finite difference method. $\mathbf{S}$ is the error covariance matrix of the solution, $\mathbf{S}_X$ is the covariance matrix of the a priori CO information, and $\mathbf{S}_\varepsilon$ is the measurement error covariance matrix. The superscript $\mathbf{T}$ represents matrix conjugate.

In these methods, we retrieved total CO column densities using the improved MOPITT CO algorithm during the periods of six months from May to October 2000. The validation results of the MOPITT retrievals of total CO column densities were good quantitative agreement with ground-based spectroscopic measurements (Drummond *et al*., 2002; Drummond and Mand, 1996). Fig. 1 shows the monthly mean of total CO column densities in the East Asian region during the periods. The spatial resolution of MOPITT output data is $0.25^\circ \times 0.25^\circ$, including latitude from 10°N to 70°N and longitude from 70°E to 170°E. In particular, we found the enhancement of total CO densities in the Asian region, and the highest density of total CO was shown in May in East Asia including China.

The enhancement of CO in East Asia may originate in the combustion of fossil fuels and the burning of biomass in springtime. In general, biomass is a major source of CO in tropical areas. Using a background tropospheric chemistry model, de Laat *et al*. (2001) showed that spatial distributions of CO emission from the two sources in China were about 10% of the global emission inventory (32.2 and 59.0 Tg CO yr^{-1}, respectively). Fang *et al*. (2001) also suggested that the forest biomass carbon storage in China between 1980 and 1998 was increased by 4.75 petagram of carbon. In addition, spatial distributions of CO emission from the burning of biomass in Indonesia and Southeast Asia include about 6.5% of the global emission inventory (de Laat *et al*., 2001). These results also agreed well with spatial distributions of high CO levels as seen in Fig. 1. The monthly mean distribution of total CO densities remained consistent except for May.

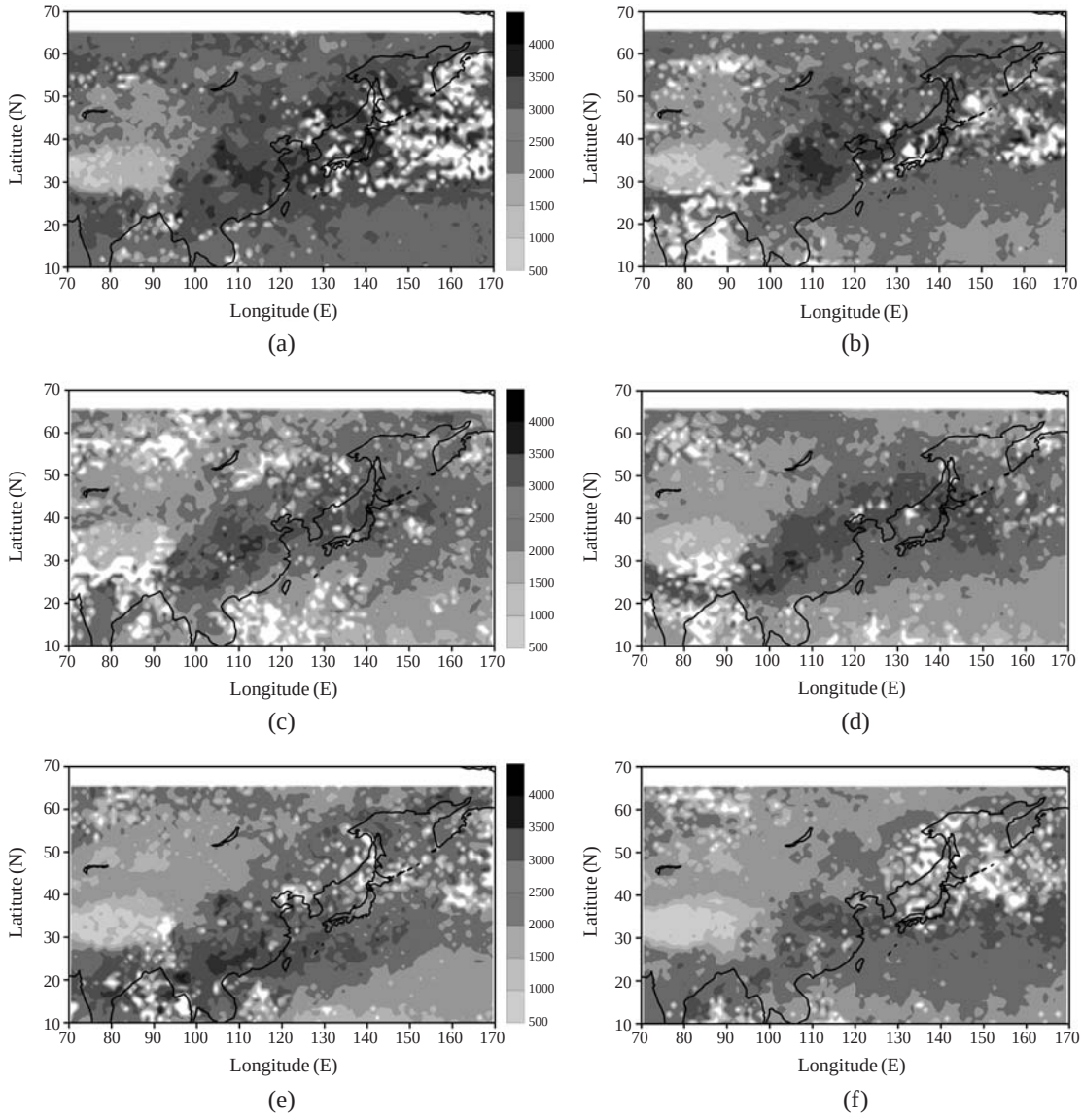

Fig. 1. Spatial distribution of total CO column density ($\times 10^{15}$ molecular/cm^2) using MOPITT from May to October 2000. (a)~(f) May, June, July, August, September, and October.

4. METEOROLOGICAL CONDITION AND ENHANCEMENT OF DAILY TOTAL CO AND OZONE

We investigated the daily data to understand enhancement of total CO densities in May in East Asia. Total CO densities increased suddenly during a weak Asian dust event in May as seen in Fig. 2. In particular, Asian dust occurs mainly in the strong westerly and travels behind cold fronts during springtime when arid regions are not covered by vegetation, and originate from the Gobi desert in Mongolia and northern China, the Taklimakan Desert in western China, and Loess plateaus in eastern China. Fig. 2 is to

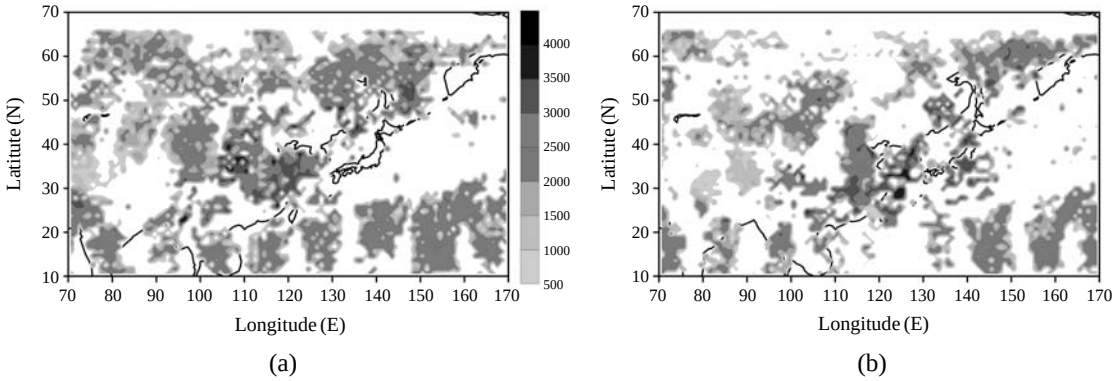

Fig. 2. Variability of total CO column density ($\times 10^{15}$ molecular/cm^2) during the period of (a) 1～3 May 2000 and (b) 4～6 May 2000 over East Asia.

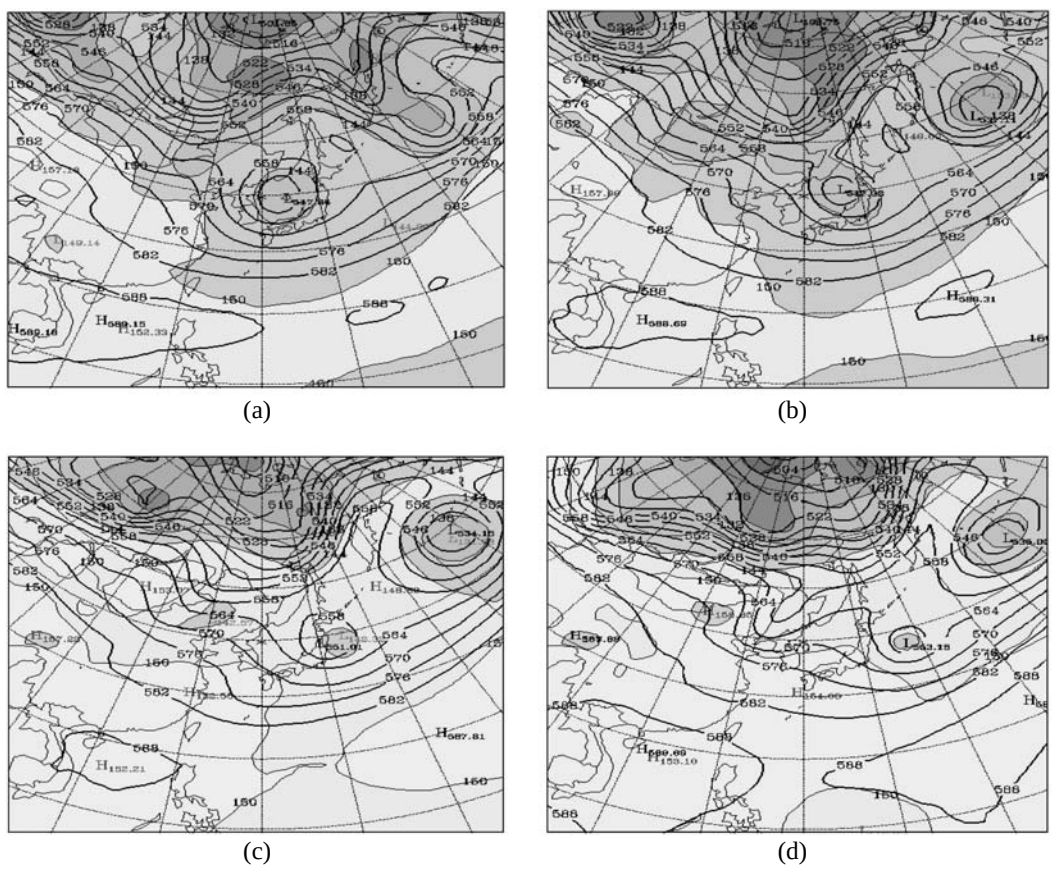

Fig. 3. Geopotential heights at 500 hPa (thick lines) and 1,000 hpa (color filled) at 1500 LST on 2～5 May 2000. (a)～(d) 2, 3, 4 and 5 May 2000.

show the daily mean variation of total CO densities of 3 days from 1 to 6 May 2000. Enhancements of total CO densities were shown in Russia, China, and subtropical areas including India and Southeast Asia, possibly originating in areas of industrial pollution and biomass burning on 1～3 May 2000. In addition, over the next three days (4～6 May 2000), total CO densities increased on the Korean peninsula, which may have been due to advection from adjacent areas, frontal transport, photochemical CO formation, surface industrial emissions, uptake by plants and biomass burning, and a deep convection downdraft associated with exchange between the free troposphere and the boundary layer.

In order to verify the origin of total CO densities, we investigated weather maps and TOMS satellite data on 1～6 May 2000, including meteorological parameters such as geopotential height and isentropic potential vorticity simulated by the final (FNL) data and the Climate Data Assimilation System (CDAS) data, respectively.

Fig. 3 shows the synoptic weather maps overlapped by both geopotential heights (thick lines) at 500 hPa and surface high and low pressure (filled colors) at 1,000 hPa in East Asia on 2～5 May 2000. Typical examples of the cut-off low are shown over Korea and the eastern Pacific. They are due to development of a strong vortex between the upper cut-off low and the surface low as they relate to the jet stream in springtime or wintertime in the mid-latitudes (Eagleman, 1985). That is, the low-pressure area at surface is connected with the low-pressure center in the upper atmosphere. This connection causes the cut-off low, which has greater wind speeds near the ground than other types of frontal cyclones. It travels very slowly, its rate of movement is the same as the dis-

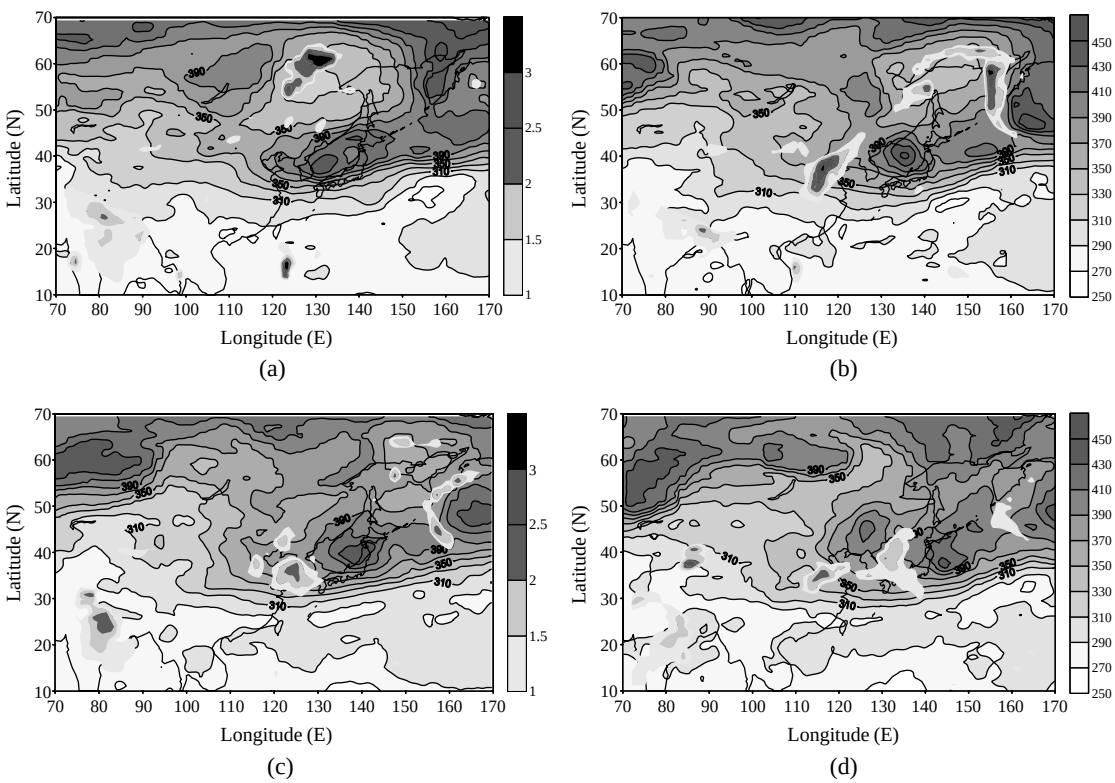

Fig. 4. TOMS total ozone (Dobson Unit, right legends) and aerosol index (left legends) in East Asia on 2～5 May 2000. (a)～(d) 2, 3, 4 and 5 May 2000.

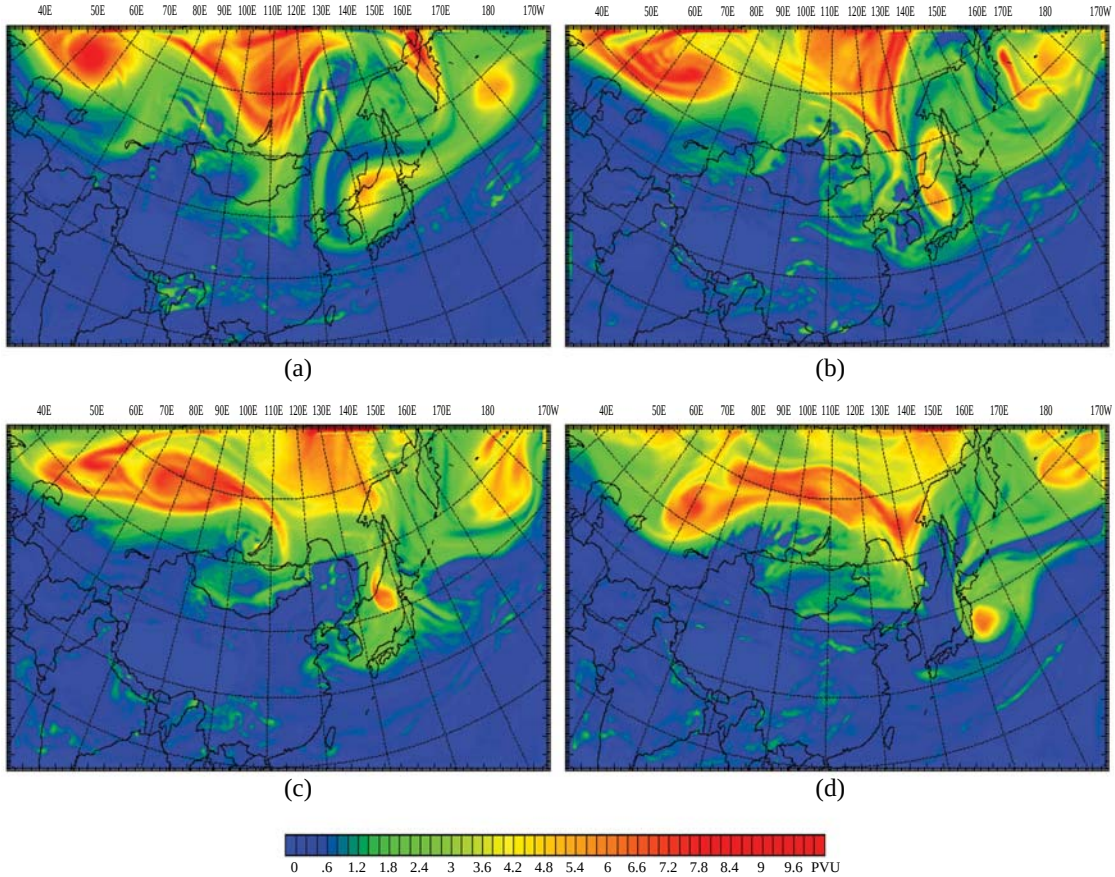

Fig. 5. Spatial distributions of the isentropic potential vorticity (IPV) in 300 K in East Asia at 1500 LST on 2～5 May 2000. (a)～(d) 2, 3, 4 and 5 May 2000.

placement speed of the whole meander in the jet stream, and it is north of the trough of the jet stream. This type of cyclone may complete a life cycle that includes the occlusion process. In Fig. 3, the cut-off low over Korea was extinguishing, but that of the eastern Pacific was developing during the given period.

The enhancements of total CO densities appear along the boundary of the surface anticyclone region behind the frontogenesis associated with the cut-off low or the surface cyclone, which is due to the whole meander in the jet stream, as shown in Figs. 2 and 3. At the same time, we discover that this is similar to the spatial distribution between geopotential heights at 500 hPa and total ozone amounts as seen in Figs. 3 and 4. The spatial distribution between the two, especially, is in good agreement with the cut-off lows. In Fig. 4, aerosol indexes show Asian dust event days. Also shown is the fact that their spatial distributions are similar to those of total CO densities located behind the surface frontogenesis related to the cut-off low or the surface cyclone. As a result, we realized that the enhancements of total CO densities were associated with movement of the cut-off lows or the surface cyclones, which was due to the jet stream during springtime. Furthermore, the cut-off lows were connected with the enhancements of total O_3 amounts.

Theoretically, the enhancement of total O_3 is relat-

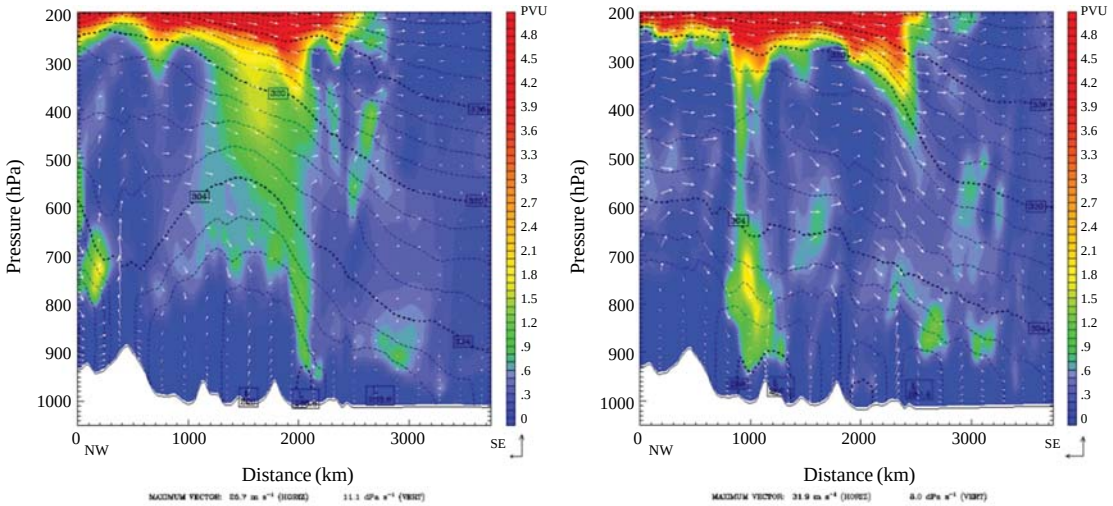

Fig. 6. Vertical cross-section along the SE (136°E, 20°N)~NW (116°E, 50°N) axis at 1500 LST on (a) 2 and (b) 3 May 2000. The vertical cross-sections includes meteorological factors such as the potential temperature (K, lines), circulation vectors between the ageostropic wind speed (m/sec) and the vertical wind speed (0.001 m/sec), and the potential vorticity (filled color).

ed to the isentropic potential vorticity (IPV), which is very useful as an indicator of the STE of ozone-rich air, and is also associated with the absolute vorticity or the cut-off low. These relationships have previously been used to estimate stratospheric contribution to air masses containing elevated ozone in the troposphere (Kim *et al*., 2002; Moon *et al*., 2002; Fenn *et al*., 1999). Ertel's isentropic potential vorticity acts as a dynamical tracer for distinguishing between the stratospheric and tropospheric air. This is given as: $IPV = -g \cdot (f+\zeta) \cdot \partial\theta/\partial p$, where $(f+\zeta)$ and $\partial\theta/\partial p$ are the absolute vorticity on an isentropic surface and the static stability, respectively, g is the gravitational acceleration, and θ is the potential temperature. Tropopause values of IPV in the mid-latitudes are generally 1.6 potential vorticity units (1 PVU$=10^{-6}$m^2/s K kg). The total ozone amount (TO) can also be expressed by integrating from the surface potential temperature (θ_s) to ∞ as a function of the cut-off low $(f+\zeta)$ to the level above the surface pressure p_s: $TO(p_s) = \int [(\chi(\theta) \cdot (f+\zeta_\theta))/(IPV(\theta) \cdot M)]d\theta$, where χ is the mass mixing ratio of ozone, and M is the ozone molecular mass. Fig. 5 represents spatial distribution of the IPV in 300 K. It shows that spatial distribution of the IPV is similar to that of geopotential height and total amount of ozone and as seen in Figs. 3 and 4.

Fig. 6 also shows vertical cross-section along the SE (136°E, 20°N)−NW (116°E, 50°N) axis, which passed through Seoul at 1500 LST on 2 and 3 May 2000. Meteorological factors such as the potential temperature (K, lines), circulation vectors between the ageostrophic wind speed (m/sec) and vertical wind speed (0.001 m/sec), and the potential vorticity (filled color) are represented along with the vertical cross-section. Stratospheric intrusions into the troposphere were observed by vertical circulation vectors as well as through values higher than 1.6 PVU, called the tropopause in the atmosphere. It was clear that the tropopause folding event, which showed potential vorticity contours dipping deep into the troposphere from the stratosphere, as seen in Fig. 6, occurred along with the cut off low during the given period. Although we did not introduce the vertical cross-section along the SE (130°E, 20°N)−NW (150 °E, 50°N) axis, which passed through the center of

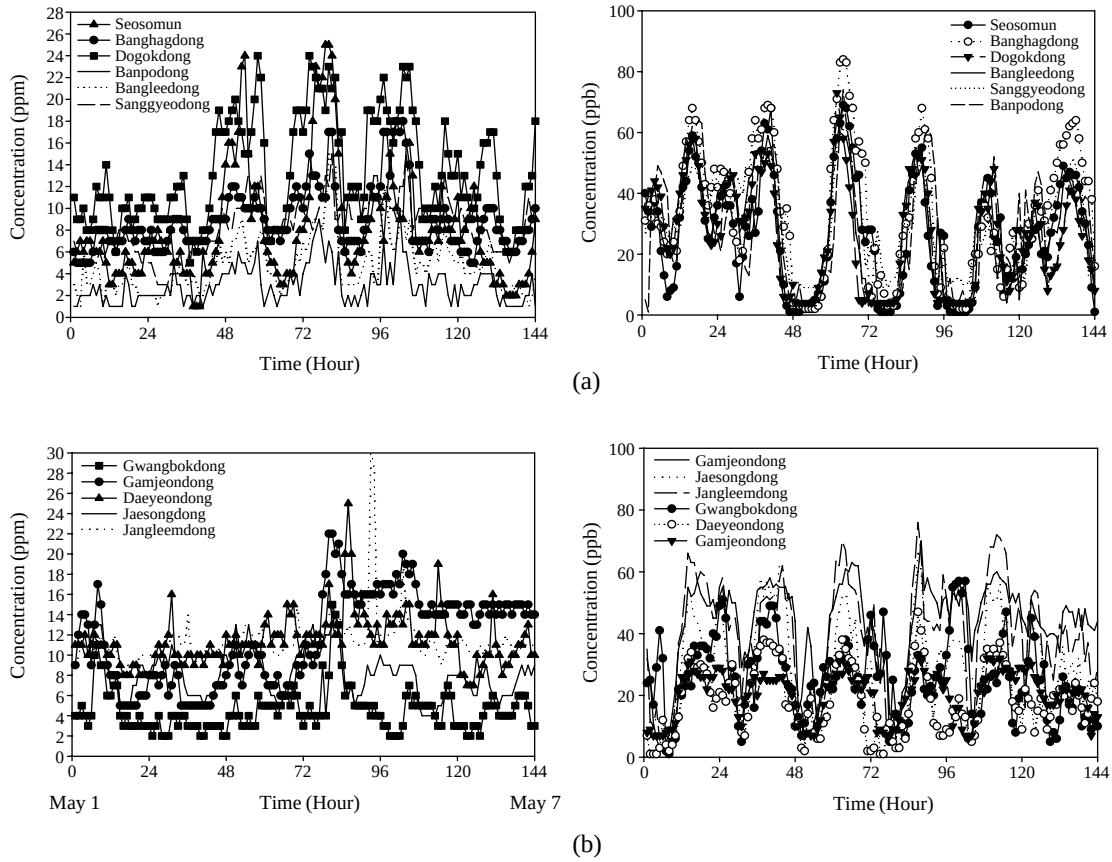

Fig. 7. Hourly variation CO (left panel) and ozone (right panel) mixing ratios at the surface air quality monitoring sites in (a) Seoul and (b) Busan, Korea during the period of 1～6 May 2000.

the cut-off low over East Asia during the same period, the tropopause folding was much stronger in this case than that which passes through Seoul. In general, it is dependent on both a very strong vorticity within the jet stream and a large thermal gradient particularly at the surface. Consequently, during the development of the cut-off low in the upper troposphere as seen in Figs. 3～6, the total ozone amount increased along the downward stretched vortex anomalies. That is, the ozone-rich air can be invaded along the elongated movement of the cut off low as a result of tropopause folding along the meandering of the jet stream over East Asia. Of course, the ozone-rich air invading the lower troposphere through circulation wind vectors, as seen in Fig. 6, can have an effect on the enhancement of surface ozone concentration.

5. ENHANCEMENT OF CO AND OZONE CONCENTRATION ON SURFACE

Above all, Asian dust moves to the Korean Peninsula under a weather condition of cut-off lows as shown in Fig. 4. Between 3 and 5 May 2000, Asian dust that occurred in the Gobi desert moved across the Yellow River, the Yellow Sea, the Korean peninsula, and the East Sea. However, the intensity of this Asian dust was weaker than that of other Asian dust events. It can also be expected that the surface enhancement of CO concentration on the Korean penin-

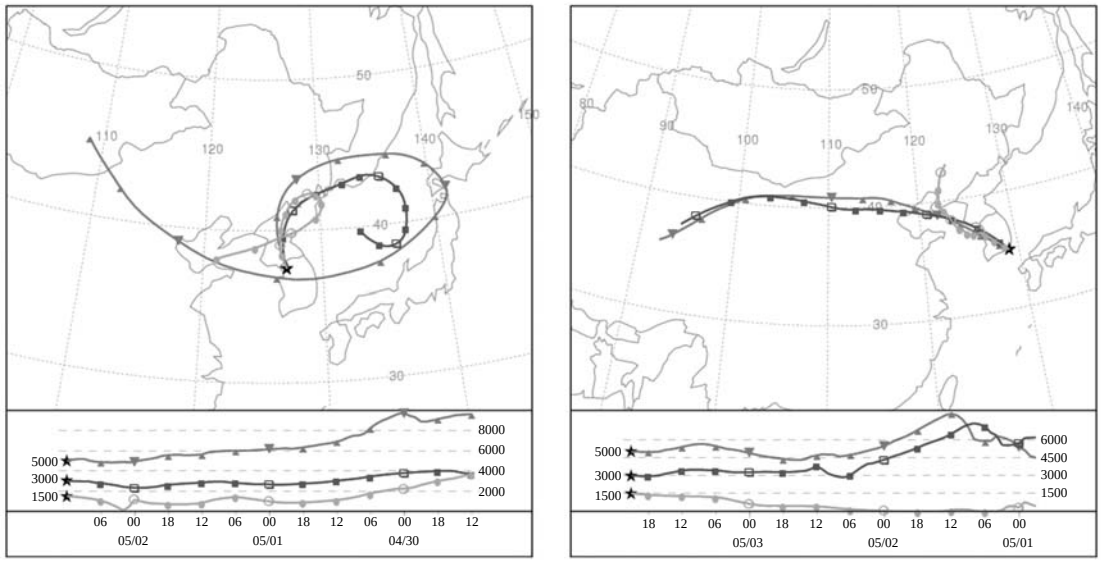

(a) (b)

Fig. 8. Backward trajectory (a) at 1200 UTC on 2 May 2000 (Seoul: 37.5°N, 127°E) and (b) at 2100 UTC on 3 May 2000 (Busan: 35°N, 129°E).

sula was partially due to long-range transport of the dust during this weak Asian dust event as seen in Figs. 2 and 4.

To identify the temporal variation of CO and O_3 related to the cut-off low, we investigated the concentration of CO and O_3 measured at each quality monitoring site in Seoul and Busan during the period of 1～6 May 2000. Fig. 7(a) shows the hourly mean concentration of CO (left panel) and O_3 (right panel) at the Seoul monitoring sites during the period, respectively. When the weak Asian dust event occurred in Seoul on May 3～5, the concentration of CO and O_3 increased suddenly in negative correlation between the two. Of particular note, it indicates that the O_3 concentration around 80 ppbv can be affected indirectly by the CO concentration because of diurnal variation, which may be presumed as the photochemical reaction of ozone precursors from local emission sources as well as their intrusion associated with the upper cut-off low in metropolitan Seoul during the episode days. However, these air quality data at Busan monitoring sites show different patterns from those of the Seoul monitoring sites as seen in Fig. 7(b). When Asian dust occurred in Busan on May 4, concentrations of CO and O_3 increased partially or weakly in an irregular relationship between the two. In this case, the O_3 concentrations were below 60 ppbv, which might be affected not by the cut-off low but the weak long-range transport.

In order to analyze the spatial origin of CO and O_3 during the period of 1～6 May 2000, backward trajectories were depicted by using the Hybrid Single-Particle Lagrangian Integrated Trajectory Model (HYSPLIT, 1997) from the final (FNL) meteorological field. Fig. 8 shows isentropic back trajectories of air parcels at 1 km, 3 km and 5 km over Seoul and Busan at 1200 UTC on May 2 and 2100 UTC on May 3, respectively. It indicates that the origins of these concentrations between the two regions are different from each other. The cut-off cyclone over Korea causes prevailing CO and O_3 concentrations in Seoul. That is, it is clear that the back trajectories over Seoul are shown along the cyclonic flow connected with the cut-off low. However those of Busan are due to long-range transport from China at all heights.

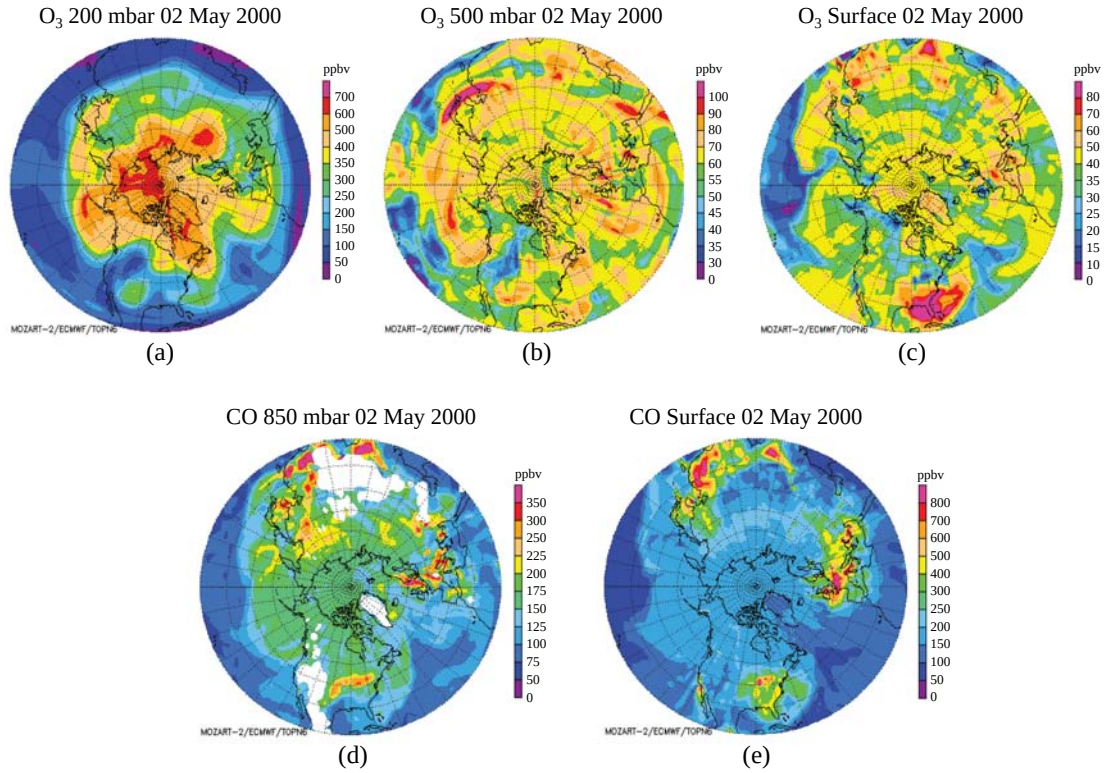

Fig. 9. Spatial distribution of O_3 and CO concentration on 2 May 2000 simulated by MOZART-2. (a)～(c) O_3 at levels of 200 hPa, 500 hPa and surface, (d)～(e) CO at levels of 850 hPa and surface.

The relative importance of chemical reactions and long-range transport of these gases in East Asia can be analyzed by using a chemical transport model incorporating the Asia emission inventory. In order to verify enhancements of CO and O_3 in Korea, we used the modeling data simulated by the Model for Ozone and Related Chemical Tracers 2 (MOZART-2), a global chemical transport model (http://www.acd.ucar.edu/gctm/), which was driven by offline meteorological fields of the European Centre for Medium-Range Weather Forecasts (ECMWF) and 2000 emission inventories during the 2001 Asia Pacific Aerosol Characterization Experiment (ACE-Asia) (Horowitz *et al*., 2003). The ACE-ASIA emission inventory includes NO_x and CO emissions from the combustion of fossil fuels and the burning of biomass. Fig. 9 shows spatial distributions of CO and O_3 simulated by MOZART-2 at levels of surface, 850, 500 and 200 hPa on 2 May 2000. The CO concentration decreased at 850 hPa but increased at surface in Korea. Consequently, it was clear that the enhancement of CO concentration in Seoul as shown in Figs. 2 and 7 was due partially to long-range transport from China in fact that the simulated data was lower than the observed data. Particularly, the O_3 concentration decreased from 200 hPa to surface over Korea. As a result, we can say that the enhancement of O_3 concentration in Seoul was due partially to intrusion from the upper troposphere as well as long-range transport from spatial distribution of O_3 concentration at each level as seen in Figs. 5, 6 and 8. Above all, in Fig. 9 (a～c), we discovered that the spatial distribution of ozone concentration was similar to that of total ozone amount related to the cut-off low over East Asia as shown in Figs. 3, 4 and 5.

Finally, during development of the cut-off low

from the tropopause into 500 hPa, the downward stretched vortex anomalies increase the amount of surface O_3 and total O_3 (see Fig. 7). At the same time, air pollutants such as CO, O_3 precursors, and aerosols located behind the frontogenesis under the cut-off low are transported by the strong westerly from China to Korea. Then the sudden daytime enhancement of ozone in the Seoul metropolitan area is expected both by the catalytic reaction of ozone precursors including CO and by the transport of ozone itself originating from a slow moving cut-off low located over Korea. Like this, severe ozone episodes in Korea often occur in the late springtime during a weak Asian dust event.

Consequently, we can understand that both the cut-off low and the surface frontogenesis in springtime play an important role in ozone episodes above 80 ppbv during a weak Asian dust event.

6. CONCLUSIONS

Recently, we have found the enhancements of total CO retrieved by MOPITT in East Asia. The spatial distribution of monthly and daily total CO column densities was the highest in East Asia in springtime when the westerly was strong and the biomass burning was active. In addition, daily total CO densities were shown behind the surface frontogenesis under the weather condition of the cut-off low related to the jet stream during a weak Asian dust event. At the same time, the weather condition of the cut-off low increased the total O_3 amount during the period. This indicates that not only ozone-rich air in the upper troposphere and stratosphere can be invaded along the elongated movement of the upper cut off low, but also O_3-precursor-rich air, including CO or dusts in the lower troposphere, can be transported along the isentropes with the surface frontogenesisby a strong westerly under the upper cut off low. In fact, such a result was obtained by indentifying the back trajectory, the isentropic vorticity, and the global chemical modeling data over East Asia.

These intrusions and transports of CO and O_3 under the cut-off low during the weak Asian dust event play an important role in metropolitan cities such as Seoul and Busan, Korea. Actually, under the weather conditions in Seoul, the enhancements of O_3 concentration were shown at about 80 ppbv during the day between 3～5 May 2000, which was due to the catalytic chemical reactions of ozone precursors including CO, as well as the intrusion of O_3 from the upper troposphere. However such phenomena in Busan were weaker than in Seoul because the region was out of the range of the cut-off low.

ACKNOWLEDGEMENTS

This work was supported by the Korea Research Foundation Grant funded by the Korean Government (MOEHRD) (KRF-2006-331-C00297).

REFERENCES

Austin, J.F. and R.P. Midgley (1994) The climatology of the jet stream and stratospheric intrusions of ozone over Japan, Atmospheric Environment, 28A, 39-52.

Cardenas, K.C., J.F. Austin, R.A. Burgess, K.C. Clemitshaw, S. Dorling, S.A. Penkett, and R.M. Harrison (1998) Correlations between CO, NO_y, O_3 and non-methane hydrocarbons and their relationships with meteorology during winter 1993 on the north Norfolk coast, U.K., Atmospheric Environment, 32A, 3339-3351.

Cicerone, R.J. (1988) How has the atmospheric concentration of CO changed? The Changing Atmosphere, J. Wiley & Sons Ltd., New York, 49-66.

Cooper, O.R., J.L. Moody, J.C. Davenport, S.J. Oltmans, B.J. Johnson, X. Chen, P.B. Shepson, and J.T. Merrill (1998) Influence of springtime weather systems on vertical ozone distributions over three North American sites, Journal of Geophysical Research, 103, 22001-22013.

Davies, T.D. and E. Schuepbach (1994) Episode of high ozone concentration at the surface resulting from transport down from the upper troposphere/lower stratosphere: A review and case studies, Atmospheric Environment, 28, 53-68.

De laat, A.T., J. Lelieveld, G.J. Roelofs, R.R. Dickerson, and J.M. Lobert (2001) Source analysis of carbon monoxide pollution during INDOX 1999, Journal of Geophysical Research, 106, 28481-28495.

Drummond, J.R. and G.S. Mand (1996) The Measurements of Pollution in the Troposphere (MOPITT) instrument: Overall performance and calibration requirements, Journal of Atmospheric Oceanic Technology, 13, 314-320.

Drummond, J.R., L. Yurganov, P. Novelli, N. Pougatchev, and F. Murcray (2002) Validation of MOPITT retrievals of carbon monoxide, 24th IGASSS (International Geoscience & Remote Sencing Symposium) 2002, Toronto, Canada, 0-7803-7537-8/02/.

Eagleman, J.R. (1985) Meteororlogy, the atmosphere in action, Wadsworth Publishing Company, 156-171.

Fang, J., A. Chen, C. Peng, S. Zhao, and L. Ci (2001) Changes in forest biomass carbon storage in china between 1949 and 1998, Science, 292, 2320-2321.

Fenn, M.A., E.V. Browell, C.F. Butter, W.B. Grant, S.A. Kooi, M.B. Clayton, G.L. Gregory, R.E. Newell, Y. Zhu, J.E. Dibb, H.E. Fuelberg, B.E. Anderson, A.R. Bandy, D.R. Blake, J.D. Bradshaw, B.G. Heikes, G.W. Sachse, S.T. Sandholm, H.B. Singh, R.W. Talbot, and D.C. Thornton (1999) Ozone and aerosol distribution and air mass characteristics over the South pacipic during the burning season, Journal of Geophysical Research, 104, 16197-16212.

Fioletov, V.E., J.B. Kerr, E.W. Hare, G.J. Labow, and R.D. McPeters (1999) An assessment of the world ground-based total ozone network performance from the comparison with satellite data, Journal of Geophysical Research, 104, 1737-1748.

Hobbs, P.V. (2000) Introduction to Atmospheric Chemistry, Cambridge University Press, Cambridge, UK, 143-163.

Horowitz, L.W., S. Walters, D.L. Mauzerall, L.K. Emmons, P.J. Rasch, C. Granier, X. Tie, J.F. Lamarque, M.G. Schultz, G.S. Tyndall, J.J. Orlando, and G.P. Brasseur (2003). A global simulation of tropospheric ozone and related tracers: Description and evaluation of MOZART, version 2 (PDF), Journal of Geophysical Research, 108 (D24), 4784.

Hubler, G., D.D. Montzka, R.B. Norton, P.C. Murphy, F.C. Fehsenfeld, S.C. Liu, B.A. Ridley, J.G. Walega, E. Atlas, F.E. Grahek, L.E. Heidt, J. Merrill, B.J. Huebert, and B.A. Bodhaine (1992) Total reactive oxidized nitrogen (NO_y) in the remote Pacific troposphere and its correlation with O_3 and CO: Mauna Loa observatory photochemistry experiment 1988, Journal of Geophysical Research, 97, 10427-10447.

Jacob, D.J. (1999) Introduction to Atmospheric Chemistry, Princeton University Press, Chichester, West Sussex, 143-163.

Khalil, M.A. and R.A. Rasmussen (1994) Global decrease in atmospheric carbon monoxide concentration, Nature, 370, 639-641.

Kim, Y.K., H.W. Lee, J.K. Park, and Y.S. Moon (2002) The stratosphere-troposphere exchange of ozone and aerosols over Korea, Atmospheric Environment, 36A, 449-463.

Kondratyev, K.Y. and C. Varotsos (2000) Atmospheric ozone variability: Implications for climate change, human health and ecosystems, Springer-Verlag Berlin Heidelberg, New York, 617pp.

Marenco, A., M. Macaigne, and S. Prieur (1989) Meridional, and vertical CO and CH_4 distributions in the background troposphere (70 N-60 S; 0-12 km altitude) from scientific aircraft measurements during the STRATOZ III experiment (June 1984), Atmospheric Environment, 23, 185-200.

Moon, Y.S., Y.K. Kim, K. Strong, S.H. Kim, Y.K. Lim, I.B. Oh, and S.K. Song (2002) Surface ozone episode due to stratosphere-troposphere exchange and free troposphere-boundary layer exchange in Busan during Asian dust events, Korean Environmental Sciences Society, 11(5), 419-436.

Novelli, P.C., K.A. Masarie, P.P. Tans, and P.M. Lang (1994) Recent changes in atmospheric carbon monoxide, Science, 263, 1587-1590

Pan, L., D.P. Edwards, J.C. Gille, M. Smith, and J.R. Drummond (1995) Satellite remote sensing of tropospheric CO and CH_4: Forward model studies of the MOPITT instrument, Apply Optics, 34, 6976-6988.

Pan, L., J.C. Gille, D.P. Edwards, and P.L. Bailey (1998) Retrieval of tropospheric carbon monoxide for the MOPITT, Journal of Geophysical Research, 103, 32277-32290.

Reichle, H.G., V.S. Connors, J.A. Holland, R.T. Sherrill, H.A. Wallio, J.C. Casas, E.P. Condon, B.B.

Gormsen, and W. Seiler (1990) The distribution of middle tropospheric carbon monoxide during early October 1984, Journal of Geophysical Research, 95, 9845-9856.

Reichle, H.G. and Coauthors (1999) Space shuttle based global CO measurements during April and October 1994, MAPS instrument, data reduction, and data validation, Journal of Geophysical Research, 104, 21443-21454

Rodrers, C.D. (1976) Retrieval of atmospheric temperature and composition from remote measurements of thermal radiation, Review of Geophysical Space Physics, 14, 609-624.

Seinfeld, J.H. and S.N. Pandis (1998) Atmospheric Chemistry and Physics: From Air Pollution to Climate Change, John Wiley & Sons, Inc., New York/ Chichester/Weinheim/Brisbane/Singapore/Tronto, p. 1326.

Smith, W.L. (1968) An improved method for calculating tropospheric temperature and moisture from satellite radiometer measurements, Monthly Weather Review, 96, 387-396.

Thompson, A.M., K.E. Pickering, R.R. Dickerson, W.G. Ellis, and D.J. Jacob (1994) Convective transport over the central United States and its role in regional CO and ozone budgets, Journal of Geophysical Research, 99, 18703-18711.

Wang, J., J.C. Gille, P.L. Bailey, L. Pan, D. Edwards, and J.R. Drummond (1999) Retrieval of tropospheric carbon monoxide profiles from high-resolution interferometer observations: A new Digital Gas Correlation (DGC) method and applications, Journal of Atmospheric Sciences, 56, 219.

Warneck, P. (1988) Chemistry of the natural atmosphere, Academic Press, New York, 131-175.

Warneck, P. (2000) Chemistry of the Natural Atmosphere, Academic Press, p. 923.

Warner, J.X., J.C. Gille, D.P. Edwards, D.C. Ziskin, M.W. Smith, and P.L. Bailey (2001) Cloud detection and clearing for the EOS Terra satellite Measurement of Pollution in the Troposphere (MOPITT) experiment, Applied Optics, 40(8), 1269-1284.

Yurganov, L.N., E.I. Grechko, and A.V. Dzhola (1995) Carbon monoxide and total ozone in Arctic and Antarctic regions: Seasonal variations, long-term trands and relationships, Science Total Environment, 160/161, 831-840.

Yurganov, L.N., E.I. Grechko, and A.V. Dzhola (1997) Variations of carbon monoxide density in the total atmospheric column over Russia between 1970 and 1995: Upward trend and disturbances, attributed to the influence of volcanic aerosols and forest fires, Geophysical Research Letter, 24, 1231-2134.